STATISTICAL DESCRIPTION OF THE INTERNAL GEOMETRY OF A POLYMER TEXTILE COMPOSITE USING MICRO-COMPUTED TOMOGRAPHY

A. Vanaerschot[1*], B.N. Cox[2], M. Blacklock[3], G. Kerckhofs[4], M. Wevers[4], S.V. Lomov[4], D. Vandepitte[1]

[1]*Department of Mechanical Engineering, KU Leuven, Leuven, Belgium*
[2]*Teledyne Scientific Co. LCC, Thousand Oaks, USA*
[3]*Department of Mechanical Engineering, University of California Santa Barbara, Santa Barbara,USA*
[4]*Department of Metallurgy and Materials Engineering, KU Leuven, Leuven, Belgium*
**Andy.Vanaerschot@mech.kuleuven.be*

Keywords: textile composite, micro-CT, probabilistic description

Abstract
The recently proposed reference period collation method, which quantifies the internal geometry of textile composites, is extended to laminated structures. Experimental data are collected for a seven-ply 2/2 twill woven carbon-epoxy composite produced by resin transfer moulding using X-ray micro-computed tomography. The data of the woven reinforcement are afterwards decomposed into non-stochastic periodic trends and non-periodic stochastic fluctuations. Each ply has systematic patterns, with exception of the in-plane centroid coordinate, that are correlated with the cross-over locations. Of the various parameters, the in-plane component of the centroid position is subjected to the largest variability.

1 Introduction

The variability of polymer composites is not yet thoroughly analysed with methods lacking for the accurate prediction of the effects of variability on the quality and reliability of composite structures [1]. When in a first step the internal geometrical scatter is quantified of a produced specimen, the effect on the mechanical properties can be evaluated in a subsequent step by constructing numerous virtual samples which have the same statistical properties as the derived statistics of the actual sample [2].

This paper characterises the internal geometrical variability over spatial scales of 1 to 15 mm using three-dimensional images acquired by X-ray micro-computed tomography (micro-CT) [3]. Use of micro-CT for quantifying geometrical variability offers advantages over the optical imaging processes, especially when spatial information needs to be analysed over the extend of a structure. Unlike optical imaging, which yields data on discrete positions in a sample [4,5], micro-CT provides information of each tow parameter for every voxel.
Quantification of scatter in geometry using micro-CT is already performed with different approaches. Desplentere et al.[6] quantified the geometrical variability of four different three-dimensional (3-D) glass fabrics. Tow dimension and spacing at certain locations are statistically quantified for measurements on the surface, by optical microscopy and X-ray micro-CT. Bale et al.[7] investigated the spatial distribution of fibre tows in two ceramic samples using synchrotron X-ray micro-computed tomography. A process of *reference period*

collation was introduced to analyse the non-stochastic periodic variations and non-periodic stochastic deviations. The tow centroid locations and tow dimensional parameters (aspect ratio, area and orientation) were analysed.

This paper extends the reference period collation method proposed by Bale et al.[7] to laminated polymer textile composites with a different topology. The objectives are to derive the geometrical information of a polymer carbon-epoxy textile laminate produced by resin transfer moulding (RTM) and to compare variability within one ply and between plies.

2 Acquisition of geometrical information

2.1 Experimental methodology

The sample material is a seven-ply polymer textile with for each ply a twill 2/2 woven carbon fabric from Hexcel (G0986 injectex) [8] with nominal unit cell dimensions of 11.4 by 11.4 mm. The dry reinforcement is impregnated with epoxy resin during a RTM production achieving a fibre volume fraction of 55.3%. The WiseTex virtual model [9] of this fabric is shown in figure 1. One unit cell has four equally spaced tows in warp and also in weft direction. The warp and weft period is labelled respectively by λ_x and λ_y.

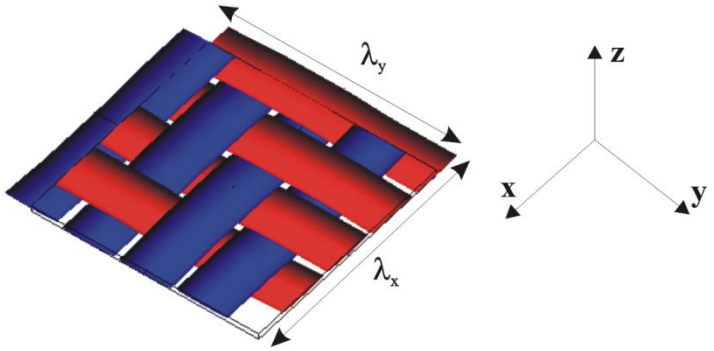

Figure 1. Virtual WiseTex model of a 2/2 twill woven fabric. The global coordinate system is also presented.

A sample of 12.5 by 12.5 mm, cut from the produced laminate, is mounted in a GE Nanotom to inspect the internal geometry. These dimensions permit analysing the geometry of one unit cell by performing one scan. The equipment has a 180 kV/15W nanofocus X-ray tube and can obtain minimum voxel sizes of 500 nm. The X-ray source parameters for this type of material and given sample size are set to 33 kV and 295 µA. 3-D images are acquired with voxel size of $(6.75\mu m)^3$.

2.2 Image analysis of high-resolution images of cross-sections

The 3-D volume representation of the composite specimen is analysed by extracting 2-D slices from this volume in each direction. The warp tow cross-sections are characterised from slices in the weft directions and weft tow cross-sections from slices in the warp direction.

The selection of the number of cross-sections to be used is based partly on the quality of the images. The carbon fibres and epoxy matrix have a similar material density and tend to give poor contrast when the voxel size is close to the fibre diameter [3]. The image quality is improved by performing subsequent post-processing filtering using the image analysis software VG Studio MAX 2.1. The noise in an image is reduced with median filters, contrast-enhancement filters and edge-preserving smoothing algorithms. Nevertheless, still locations in the image exist where the boundary between a warp and a weft tow are hard to distinguish. Figure 2 presents such a processed cross-sectional image.

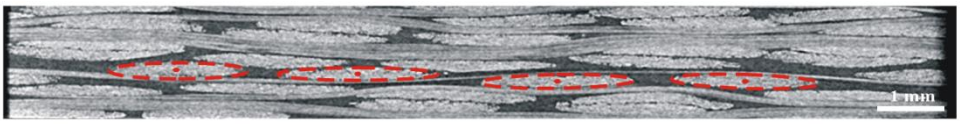

Figure 2. Digital image of a cross-section in weft direction obtained by micro-CT. The quality of the image is improved by subsequent post-processing steps.

The presence of blurry boundaries demands for a manual input in the image segmentation to analyse the reinforcement structure. The analysis of the internal structure of the specimen is therefore limited to nineteen slices both in warp and weft direction. Given the unit cell dimensions, each tow cross-over contact is inhabited by three data slices in each direction. Image segmentation is performed separately for warp and weft slices with the Avizo v6.1 software (software licence Lawrence Berkeley National Laboratory, Berkeley, CA, USA). Each tow is characterised by fitting ellipses to the tow cross-sections using the freeware ImageJ, with the principle shown in figure 2. For each image slice, the tow path centroid (x,y,z), tow aspect ratio AR, tow area A and tow orientation θ of its cross-section are quantified. A set of images is sufficient to fully characterise the tow path over the entire length of the tows.

2.2 Transformation to global coordinate system and sample alignment correction

The tow data is affected by the inevitable misalignment of the sample in the Nanotom during the scan. All tow data are converted to the global material coordinate system of figure 1, with the x-axis as warp direction and y-axis as weft direction. An optimisation technique is used to correct for the misalignment of the sample and extract the unit cell dimensions. From this information, also the shear angle and ply angle are derived. The average results over all plies are summarised in table 1.

	λ_x [mm]	λ_y [mm]	Ψ [°]	ϑ [°]	t_p [mm]
Mean	11.55	11.48	90.37	-1.38	0.43
σ	0.22	0.36	2.03	1.26	0.03
cv [%]	1.92	3.11	2.24	-	6.44

Table 1. Average geometrical characteristics of the plies

The periodic length is similar for the warp and weft direction, as is expected for this balanced fabric, with the weft direction exhibiting a slightly higher coefficient of variation *cv*. The ply angle ϑ, defined as the average orientation of the warp tows in each ply, and shear angle ψ only show mild variations between the plies. The thickness of each ply t_p is calculated as the difference between the lowest and highest z-coordinates of all tows within that ply. Neighbouring plies show overlapping z-coordinates at different locations in the xy-plane due to the nesting of the plies. A quantification of this nesting can be obtained by summing the ply thicknesses and divide it by the laminate thickness, resulting in a nesting value of 1.40. Nesting will have an effect on the statistical behaviour of the tow path.

3 Statistical analysis of the tow paths

The reference period collation procedure uses the concept of *tow genus* to assign tows that should be identical [7]. Considering the weaving process for the considered 2/2 twill woven fabric, all warp tows can be represented by one tow genus and all weft tows by another tow

genus. Distinct genuses are introduced for warp and weft tows for each plies to compare the systematic and stochastic behaviour of neighbouring plies.

3.1 Reference period definition

A reference period λ_i is selected for each tow genus. On this period, a uniform grid is chosen with sixteen grid points and grid spacing δ accordingly chosen to the number of slices per period. The procedure is shown in figure 3. The tow dataset can be presented by five parameters $\{\rho_i^{(j,t,p)}, z_i^{(j,t,p)}, AR_i^{(j,t,p)}, A_i^{(j,t,p)}, \theta_i^{(j,t,p)}\}$ with ρ= y for warp tows and x for weft tows. Data are given for each grid location *i*=1...16, tow label *j*=1...4 within the tow genus set *t*=warp or weft and ply *p*=1...7.

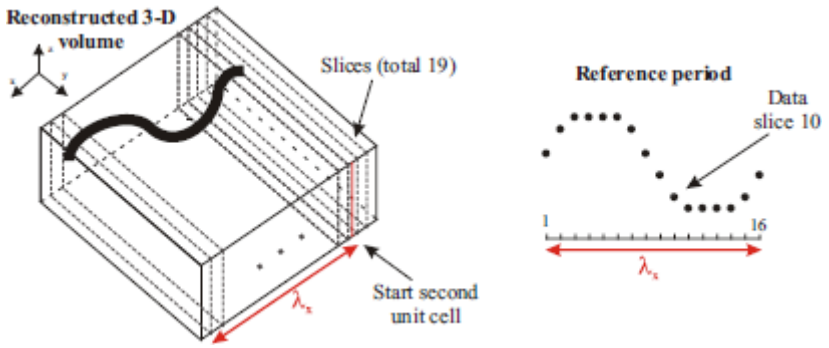

Figure 3. Procedure of reference period collation for the current case of nineteen analysed slices.

The tow path is statistically analysed by partitioning each of the characteristics into periodic systematic variations and non-periodic stochastic deviations. For ε representing one of the five parameters:

$$\varepsilon_i^{(j,t,p)} = < \varepsilon_i^{(j,t,p)} > + \epsilon_i^{(j,t,p)} \quad (1)$$

with $\epsilon_i^{(j,t,p)}$ the zero-mean deviation from the systematic value $< \varepsilon_i^{(j,t,p)} >$ at location *i* along the tow *j* of the tow genus *t* in ply *p*. This process uses a Hermite interpolation scheme to calculate the parameter values at each grid location since their locations do not coincide with those of the nineteen slices (see figure 3). This interpolation polynomial is also used to determine the cross-over locations where warp and weft tows have equal centroid locations in the xy-plane.

3.2 Systematic trend of the tow path

The systematic trend of each tow is identified using all available data. Tows with equal genus classification are translated to the reference period using the vector $(\frac{m\lambda_x}{4}\boldsymbol{e_x} + \frac{n\lambda_y}{4}\boldsymbol{e_y})$ with m and n integers. The systematic variation $\mu_i^{(t,p)}$ of each tow genus is obtained by

$$\mu_i^{(t,p)} = \frac{1}{N_i}\sum_j \left[\varepsilon_i^{(j,t,p)} - \left(m\frac{\lambda_x}{4}\boldsymbol{e_x} + n\frac{\lambda_y}{4}\boldsymbol{e_y}\right)\right] \quad (2)$$

with $\boldsymbol{e_x}$ and $\boldsymbol{e_y}$ the unit vectors and N_i the number of data points belonging to the grid location *i*.

3.3 Statistical properties of the tow path

For each single genus, all the deviations of the parameters from their systematic values can be used to (i) determine the standard deviation of the deviations for any parameter and (ii) evaluate the correlations existing between the parameter values within one tow.

The standard deviation is defined for each parameter combining the data for all grid locations *i* and for each tow *j* belonging to the genus *t* and assuming that it is independent of the grid point location:

$$\sigma_{\epsilon}^{(t,p)} = \frac{\sqrt{\sum_{i,j}\left(\epsilon_i^{(j,t,p)}\right)^2}}{N-1} \tag{3}$$

with *N* the size of the dataset used for calculating the standard deviation.

Correlations along a tow are calculated using the Pearson's correlation parameter for pairs of data $\{\varepsilon_i^{(j,t,p)}, \varepsilon_{i+k}^{(j,t,p)}\}$ taken from different locations on the same tow spaced by kδ. The autocorrelation coefficient is determined by

$$C^{(j,t,p)}(k) = \frac{\sum_{i=1}^{n-k} \varepsilon_i^{(j,t,p)} \varepsilon_{i+k}^{(j,t,p)}}{\sqrt{\sum_{i=1}^{n-k} \varepsilon_i^{(j,t,p)^2}} \sqrt{\sum_{i=1}^{n-k} \varepsilon_{i+k}^{(j,t,p)^2}}} \tag{4}$$

with *n* the number of pairs and *k* an integer value. This coefficient is used to determine the correlation length. For each tow genus, this parameter is defined by fitting a straight line to the variation of the correlation parameter, using data for small *k*:

$$C^{(j,t,p)}(k) \approx 1 - k\delta/\xi^{(j,t,p)} \tag{5}$$

with $\xi^{(j,t,p)}$ the correlation length. This linear fit only uses the first five datapoints (k ≤ 5). Higher spacings have correlation values which are based on a much smaller dataset and therefore inappropriate for evaluating the correlation length.

4 Results of the statistical analysis with comparison between plies

4.1 Results for the systematic variations

The systematic variations are first defined for all individual plies using distinct warp and weft genuses. This calculation provides a mean warp and weft genus for each ply. The systematic curves obtained with distinct warp and weft genuses defined for different plies can subsequently be compared to check whether significant differences are present between plies. The similarity is quantified by translating each ply systematic genus to the reference period. The mean value at each position along the tow is computed:$< \varepsilon^{(t,m)} >$. The difference between the systematic curve for any single ply *p* and the mean systematic curve is then characterised by the parameter $\delta^p = \sqrt{\int_i \left(< \varepsilon_i^{\{(t,p)\}} > - < \varepsilon_i^{\{(t,m)\}} >\right)^2 dx}$. This procedure is shown in figure 4 for the warp out-of-plane coordinate. Table 2 presents the difference measure δ^p for each ply systematic curve relative to the mean systematic curve.

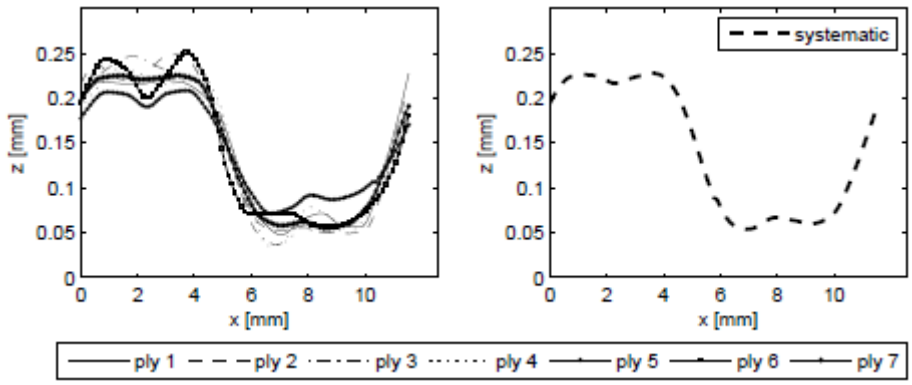

Figure 4. Systematic trends for distinct plies translated to one reference period (left) and the overall mean systematic curve (right).

	δ_x^p [mm]	δ_y^p[mm]	δ_z^p[mm]	δ_{AR}^p[-]	δ_A^p[mm²]	δ_θ^p[°]
Warp tows	-	0.027	0.012	0.817	0.014	0.680
Weft tows	0.024	-	0.014	1.110	0.017	0.996

Table 2. Difference measure between the systematic curves for individual plies

The difference measure for any parameter and for any ply is less than the standard deviation of the stochastic variations of that parameter within a single ply. Therefore, the plies are approximately indistinguishable except for the present *dip* in the out-of-plane coordinate. This feature is a plausible result of the compaction and mutual interaction of tows during production. The surface plies do not exhibit dips, which might be attributed to the presence of flat platens in the moulding process to which the surface plies conform. This dip is the only difference observed between the systematic curves for the different plies. The systematic variations of aspect ratio, area and orientation computed for a weft genus are correlated with the locations of the cross-overs, as is presented in figure 5.

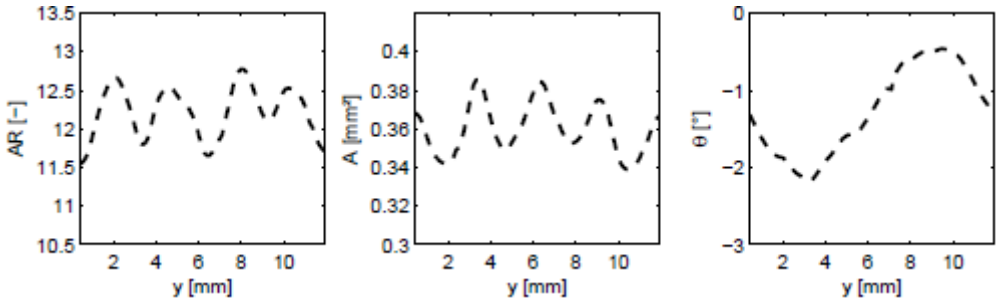

Figure 5. Systematic curves for the warp tow dimensional parameters.

4.2 Results for the stochastic deviations

The deviations from the systematic trend are first analysed using a distinct genus for each ply. Since no significant differences were observed between all the deviations, whatever ply they belong to, further analyses of deviations were carried out combining warp or weft tows from all plies into two distinct genuses. The combination of all the warp deviations in one dataset and all weft deviations in another dataset also demonstrates that the deviations are normally distributed. The standard deviations computed for all parameters are presented in table 3. The in-plane centroid coordinates for both warp and weft genuses have the largest deviations. This is expected since the in-plane path is not as restricted as the out-of-plane path during RTM production.

	σ_x [mm]	σ_y [mm]	σ_z [mm]	σ_{AR} [-]	σ_A [mm²]	σ_θ [°]
Warp genus	-	0.113	0.014	1.774	0.023	0.797
Weft genus	0.063	-	0.015	1.440	0.024	0.833

Table 3. Standard deviations of each tow parameter considering the data of all plies for each type of tow

4.3 Correlation lengths for the tow parameters deviations

The autocorrelation of each component is determined, first using distinct genuses for tows in each ply and then combining the tows of one type from all plies into single genuses. Figure 6 shows the Pearson's correlation parameter in function of the separation of two points on a tow, for the warp z-coordinate and y-coordinate. The data for one single genus combining the data from all plies are presented by circles and the data for genuses defined for individual plies by lines. The autocorrelation graph for the z-coordinate deviations indicates correlation lengths in the range of 2-4 mm. The y-coordinate graph shows much larger correlation lengths, exceeding the unit cell dimensions. Table 4 shows the correlation length for the data combining all the tow information.

	ξ_x [mm]	ξ_y [mm]	ξ_z [mm]	ξ_{AR} [mm]	ξ_A [mm]	ξ_θ [mm]
ξ^{warp}	-	22.12	1.55	7.17	2.43	4.49
ξ^{weft}	9.29	-	1.67	5.16	0.91	3.48

Table 4. Correlation lengths for the different tow parameter

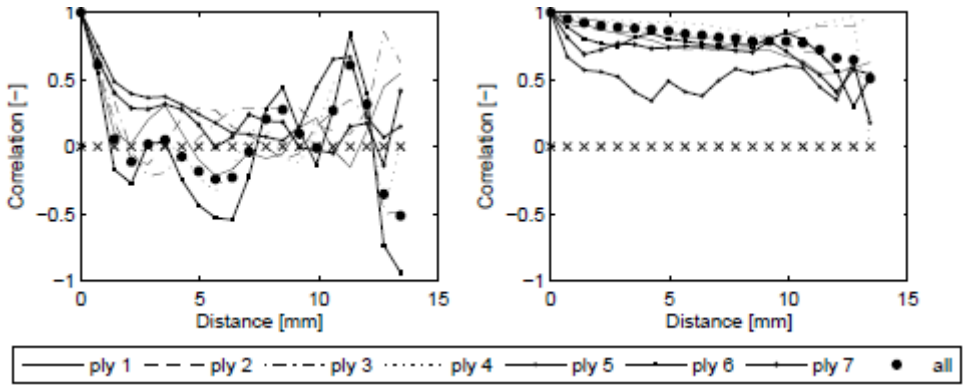

Figure 6. Autocorrelation graph for the out-of-plane centroid coordinates (left) and the in-plane centroid (right).

The correlation lengths of the out-of-plane centroid coordinates are smaller than the cross-over spacing in the weave, as was observed in [7]. This is caused by the inter-ply nesting effects. The same conclusion is made for the correlation length of the area. The in-plane centroid coordinate has correlation lengths which exceed the unit cell dimensions for the warp genus. Thus a long-range deviation is present for this displacement component, which must be investigated on larger samples. The correlation lengths for the tow parameters of orientation and aspect ratio are within the unit cell size. The aspect ratio has slightly higher correlation length.

5 Conclusions

The reference period collation method can be extended to laminated, nested structures by modifying the manner in which tows are grouped into genuses. Further, the geometrical variability of the considered high-performance carbon-epoxy composite is found to be significant. The tow parameters have systematic curves that depend on the cross-over

locations, with exception of the in-plane coordinate. No major differences are observed in this mean behaviour between the different plies, indicating a minimal effect of the random nesting of plies. The in-plane centroid coordinate is subjected to the largest variability from its systematic curve and their deviations are also correlated over relatively long distances along the tow axis, exceeding the unit cell size. The deviations from systematic patterns are also similar for all plies, no significant inter-ply effects are observed. Additional data need however to be collected to reduce the uncertainty in the stochastic characteristics. The statistics reported here will serve as input for numerical modelling strategies of composite materials. They are the calibrating data for generating virtual samples that possess the same stochastic properties as those computed for the experimental samples.

Acknowledgements
This work was made possible by the financial support of the Flemish Government through FWO-Vlaanderen and the Agency for Innovation by Science and Technology in Flanders (IWT). This support is gratefully acknowledged.

References

[1] Charmpis D.C., Schuëller G.H., Pellisetti M.F. The need for linking micromechanics of materials with stochastic finite elements: A challenge for materials science. *Computational Materials Science*, **41**, pp. 27-37 (2007).
[2] Blacklock M., Bale H., Begley M., Cox B. Generating virtual textile composite specimens using statistical data from micro-computed tomography: 1D tow representations for the Binary Model. *Journal of the Mechanics and Physics of Solids*, **60**, pp. 451-70 (2012).
[3] Landis E., Keane D. X-ray microtomography. *Materials Characterization*, **61**, pp. 1305 16 (2010).
[4] Lomov S., Belov E., Bischoff T., Ghosh S., Thanh T., Verpoest I. Carbon composites based on multi-axial multi-ply stitched performs. Part 1: Geometry of the perform. *Composites Part A*, **33**, pp. 1171-83 (2002).
[5] Olave M., Vanaerschot A., Lomov S., Vandepitte D. Internal geometry variability of two woven composites and related variability of the stiffness. *Submitted to Polymer Composites* (2012).
[6] Desplentere F., Lomov S.V., Woerdeman D.L., Verpoest I., Wevers M., Bogdanovich A. Micro-CT characterization of variability in 3D textile architecture. *Composites Science and Technology*, **65**, pp. 1920-30 (2005).
[7] Bale H., Blacklock M., Begley M., Marshall D., Cox. B., Ritchie R. Characterizing three-dimensional textile ceramic composites using synchrotron X-ray micro-computed-tomography. *Journal of the American Ceramic Society*, **95**, pp. 392-402 (2012).
[8] Hexcel. *HexForce G0986 SB 1200* (2012).
[9] Verpoest I., Lomov S.V. Virtual textile composites software WiseTex: Integration with micro-mechanical, permeability and structural analysis. *Composites Science and Technology*, **65**, pp. 2563-74 (2005).